



Microstructure and Corrosion Behavior of Aluminum Coatings Prepared by High-Efficiency Supersonic Plasma Spraying and Oxygen–Acetylene Flame Spraying

Zi-ang Jin¹ · Ming Liu² · Li-na Zhu^{1,4} · Hai-dou Wang^{1,2} · Guo-zheng Ma² · Zhi-guo Xing² · Jia-jie Kang^{1,4} · Shu-ying Chen³

Submitted: 27 August 2019 / in revised form: 2 January 2020
© ASM International 2020

Abstract Thermal spraying aluminum coatings have been widely used in the corrosion protection of mild steel in seawater. In this study, high-efficiency supersonic plasma spraying (HESP) and oxygen–acetylene flame spraying (FS) were used to prepare aluminum coatings. The micromorphology of the coatings was analyzed by a scanning electron microscope equipped with an energy-dispersive x-ray spectrometer. The phase identification of the coatings was conducted by an x-ray diffractometer. The Vickers hardness and bonding strength of the coatings were measured by an HMV-2000 Vickers hardness tester and MTS809 universal tensile tester. The corrosion resistance of the coatings was tested by an IM6ex electrochemical workstation. The results show that the aluminum coatings prepared by HESP have a denser structure, higher micro-hardness, higher bonding strength, and better corrosion resistance than those prepared by the traditional FS. After 480-h immersion in 3.5 wt.% NaCl solution, a dense corrosion product formed on the surface of aluminum coatings prepared by HESP prevents further corrosion of the

coatings, but the aluminum coatings sprayed by FS demonstrate a serious pitting phenomenon.

Keywords aluminum coatings · corrosion resistance · mechanical property · microstructure

Introduction

In marine environments, serious corrosion problems exist in the interior and outboard structures of ships, offshore platforms, and port facilities. Spraying metal protective coatings is an important means to solve the long-term protection of steel structures in marine environments (Ref 1-4).

Aluminum is a kind of good anode material that has a higher negative electrode potential than steel. In the presence of electrolyte, aluminum coatings can protect the cathode by sacrificing the anode (Ref 5, 6). Moreover, when immersed in 3.5 wt.% NaCl solution, the aluminum coating can generate stable water-insoluble corrosion product, Al(OH)₃. The dense corrosion product can effectively prevent the corrosion medium from infiltrating into the coating, which has a good isolation and protection function (Ref 7). In order to evaluate the corrosion resistance of aluminum coating, Esfahani et al. (Ref 8) carried out electrochemical impedance spectroscopy (EIS) and polarization tests in 3.5 wt.% NaCl solution. The results showed that the corrosion resistance of the coating was improved because the corrosion products blocked the pores of the coating and prevented the electrolyte from penetrating into the coating. Zhang et al. (Ref 9) sprayed a layer of aluminum coating on the surface of Q235 steel by oxy-acetylene flame spraying. After soaking the substrate and aluminum coating in the 3.5 wt.% NaCl solution for 120 h,

✉ Li-na Zhu
zhulina@cugb.edu.cn

✉ Hai-dou Wang
wanghaidou@aliyun.com

¹ School of Engineering and Technology, China University of Geosciences (Beijing), Beijing 100083, China

² National Key Lab for Remanufacturing, Academy of Armored Forces Engineering, Beijing 100072, China

³ National Key Laboratory of Human Factors Engineering, China Astronaut Research and Training Center, Beijing 100094, China

⁴ Zhengzhou Institute, China University of Geosciences (Beijing), Zhengzhou 451283, China

it was found that the corrosion of aluminum coating was slight, which indicated that the aluminum coating could well-prevent steel from corrosion.

Thermal spraying is a kind of material forming technology that uses flame, arc, plasma arc, and other heat sources to heat the spraying material to the melting state, accelerating the melting spraying particles at the same time, and spraying them to the surface of the pretreated substrate to form the coating (Ref 10). For the spraying of aluminum coatings, the traditional thermal spraying technologies, such as flame spraying and arc spraying, were mostly used. Zlatko et al. (Ref 11) used the method of response surfaces to study the bonding strength of aluminum coatings sprayed by flame spraying technology, and the maximum value of bonding strength between coatings and substrate was 22.45 MPa. Malek et al. (Ref 12) studied the performance of 99.5 wt.% aluminum coating sprayed by arc spraying technology, and the results showed that the bonding strength between coatings and substrate was 12.38 MPa. Rodriguez et al. (Ref 13) compared aluminum coatings deposited by flame spraying and arc spraying methods, and the results showed that the porosities varied in the range of 3-7% for flame-sprayed coating and 1-7% for arc-sprayed coating. Although the traditional thermal-sprayed aluminum coatings have been widely used for corrosion protection of low carbon steel, it is a fact that some problems, such as the presence of many internal pores, coating looseness, and low bonding strength between coatings and substrate, exist in coatings (Ref 14-18). Long-term immersion in seawater will lead to the early separation of coatings and substrate, and more pores will lead to the penetration of corrosive medium into the coatings to accelerate the corrosion of the coatings and reduce the thickness of the coatings. These defects can seriously affect the corrosion protection duration of the aluminum coating on mild steel, which cannot meet the increasingly stringent requirements for the long-term protection of mild steel.

HESP, as an important thermal spraying technology, has the following advantages: (1) the jet temperature can be adjusted in a wide range (1000-10,000 °C), which can be used to spray aluminum coating; (2) the spray particles have a high flying speed (400-600 m/s), which can be spread evenly when they are sprayed to the substrate; (3) the internal powder feeding nozzle is used, which has a high deposition efficiency; (4) the argon is used as inert ionization gas, which results in low oxidation degree of particles, less defects, and good quality of coatings. Therefore, compared with the traditional thermal spraying technology, HESP can obtain high-quality coatings, which has a broad application prospect in engineering (Ref 19).

In this study, aluminum coatings were prepared by HESP and FS. The quality, mechanical properties, and corrosion resistance of the two coatings were studied and compared.

Experimental Materials and Methods

Experimental Materials

The substrate is AISI 1045 steel with a size of 70 mm × 10 mm × 3 mm. The spraying raw materials were aluminum powders (purity ≥ 99.7%) produced by Beijing Sangyao Technology Development Co., Ltd., China, and their morphologies are shown in Fig. 1. The powders were mainly spheroidal, and the particle size distribution range was 15-45 μm.

Preparation of Aluminum Coatings

Prior to spraying, aluminum powders were dried for 3 h at 100 °C in the drying oven to prevent them from getting wet. The substrate AISI 1045 steel, whose sides had a chamfer with length of 1 mm and an angle of 45°, was cleaned ultrasonically for 30 min in a bath of alcohol to remove oil stains. Then, the substrate surface was grit-blasted by a manual blasting machine, using 500 μm angular alumina grits. The distance and angle of grit blasting were 200 mm and 90°, respectively. Finally, the aluminum coatings were fabricated by FS and HESP developed by National Key Laboratory for Remanufacturing, China. The HESP system is shown in Fig. 2, and process parameters of grit blasting and spraying are given in Table 1.

Characterization of Aluminum Coatings

The microstructure and composition of the coatings were analyzed by a Nova NanoSEM50-type environmental scanning electron microscope (SEM, FEI, America), which was equipped with an x-ray spectrometer (EDS, Oxford, England). The phase composition was conducted by x-ray diffractometer (XRD, Bruker, Germany) with Cu K α radiation. The tube voltage and current were 40 kV and 150 mA, respectively. The scanning speed was 3°/min, and the range was 20°-90°.

The porosity of the coating was calculated by the gray scale method. The main steps were as follows: take 10 photographs of 800× magnification SEM at different positions of the coating cross section, input the photographs into ImageJ2x software to process them as grayscale images, then calculate the coating porosity of each photograph, and take the average value.

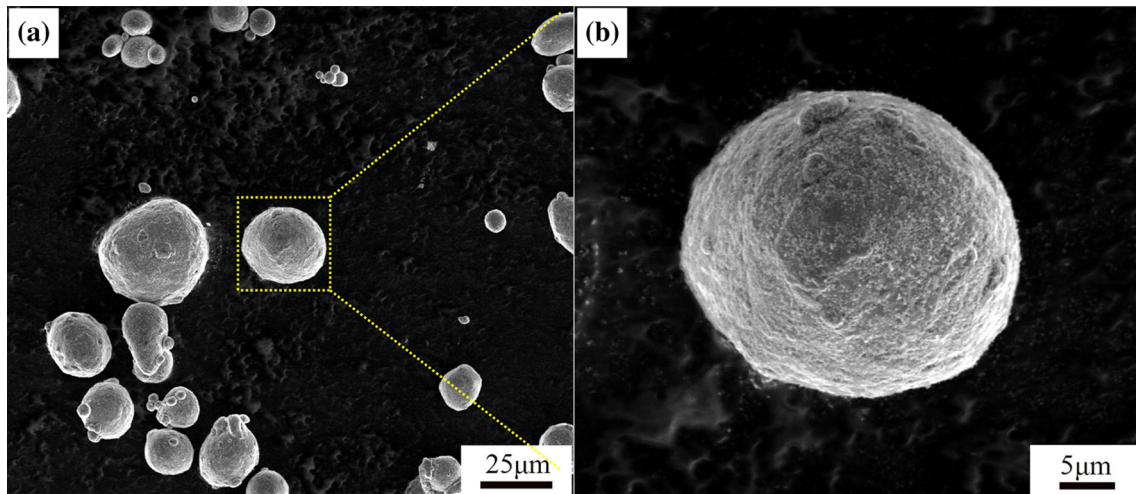


Fig. 1 Microscopic morphology of aluminum powders: (a) low magnification; (b) high magnification

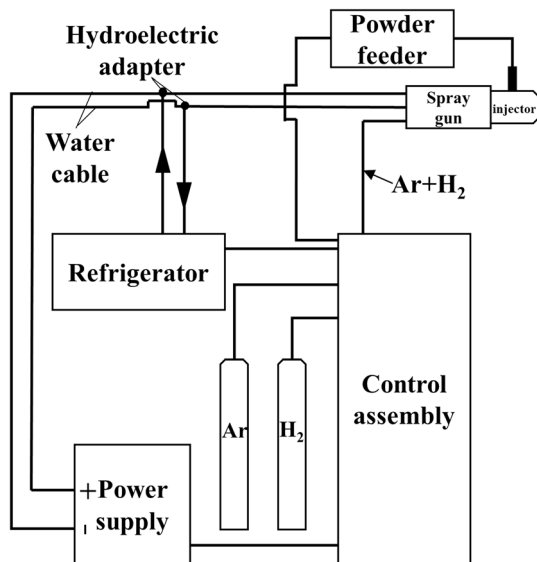


Fig. 2 High-efficiency supersonic plasma spray system

Table 1 Grit blasting and spraying parameters

Process	Parameters	Values
Grit blasting	Air pressure (MPa)	0.7
	Blasting distance (mm)	300
	Blasting angle (°)	90
HESP	Voltage (V)	130
	Current (A)	350
	Spraying distance (mm)	100
	Cooling of substrate	Air blow
	Gas flow rate (L/min)	Ar(120), H ₂ (13)
	Coating thickness (mm)	0.30
FS	Oxygen pressure (MPa)	0.75
	Oxygen flow rate (L/h)	500
	Acetylene pressure (MPa)	0.8
	Acetylene flow rate (L/h)	1000
	Spraying distance (mm)	160
	Coating thickness (mm)	0.30

The microhardness of coatings was measured using a microhardness tester (MICROMET-6030, Buehler, America) with a load of 100 gf and hold time of 15 s. The microhardness values were the average of 10 measurement points to eliminate the artificial disturbance effects.

The microhardness of coatings was measured by the microhardness tester (MICROMET-6030, Buehler, America). The test parameters were load 100 gf and hold time 15 s. The bonding strength between coatings and substrate was tested by an MTS809 universal tensile testing machine. According to ASTM C-633-01 standard, the cross-head speed of the equipment was 1 mm/min. The bonding strength is the average of three measurements. The tensile test specimen is shown in Fig. 3.

Corrosion Tests

Electrochemical impedance spectroscopy (EIS) and Tafel polarization measurements were performed using a conventional three-electrode system (in Fig. 4). The working electrode was the test sample with an effective area of 1 cm²; the platinum was the counter electrode; the reference electrode was the saturated calomel electrode (SCE); and the corrosive medium was a 3.5 wt.% NaCl solution (pH = 7). The Tafel polarization curves and the EIS spectra measurement were all performed on the electrochemical workstation (IM6ex, Zahner, Germany). The polarization curves were fitted with CorrView 2 software, and the impedance spectra were analyzed with ZSimpWin 3.21

software. The Tafel polarization curve has a scanning speed of 1 mV/s and a scanning range from -300 to 600 mV (relative to the open circuit potential). The EIS spectra were measured at an open circuit from the corrosion potential, the excitation voltage signal amplitude was 5 mV, and the test frequency range was 10^5 - 10^{-2} Hz.

Results and Discussion

Micromorphology and Composition of Aluminum Coating

The surface morphology of aluminum coatings sprayed by HESP and FS is shown in Fig. 5. It can be seen from

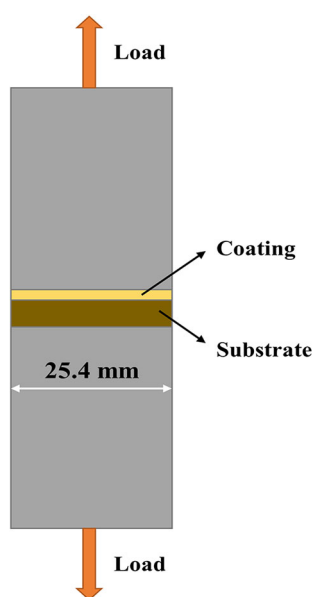


Fig. 3 Tensile test specimen for measuring bonding strength of spray coatings

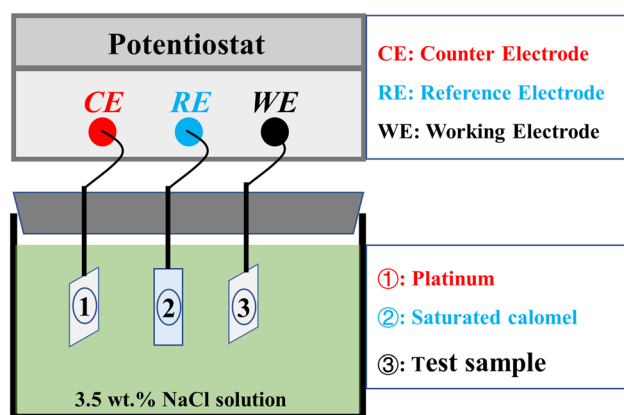


Fig. 4 Schematic diagram of three-electrode system

Fig. 5(a) that the surface of the aluminum coating sprayed by HESP is relatively flat, and there are fewer unmelted spherical particles, which indicates that the particles have fully melted and spread evenly on the surface of the substrate. On the contrary, in Fig. 5(b), there are many spherical and striped particles in the surface of the aluminum coating sprayed by FS, indicating that the particles are not fully melted. It can also be seen from Fig. 5(b) that there are many pores in the accumulation position of particles, which indicates that the formation of pores in the coating is mainly due to the inclusion of unmelted spherical and strip particles in the coating, forming pores around them.

The cross section morphologies of the aluminum coatings sprayed by HESP are shown in Fig. 6(a) and (b). The coating is very dense, with only a few micropores, no cracks, unmelted particles, and other defects. However, compared to the aluminum coatings sprayed by HESP, more voids, unmelted particles, and cracks are present on the aluminum coatings sprayed by FS (Fig. 6c and d). There are also pores and cracks at the interface between the FS-sprayed coatings and substrate, which will result in lower bonding strength. The porosities of the aluminum coatings sprayed by HESP and FS are 1.02 and 2.18%, respectively. This is because, compared to FS, HESP has the characteristics of better particle melting state and higher flight speed of particles, which makes particles have higher kinetic energy and heat energy. When the particles were sprayed on the substrate, the flattening of the particles is more sufficient and the spreading is more uniform, which makes the coating more compact.

The XRD pattern of the aluminum coatings sprayed by HESP and FS is shown in Fig. 7. The phase compositions of the two sprayed aluminum coatings are pure aluminum, and there are no other secondary phases.

Mechanical Properties of Aluminum Coatings

The microhardness and bonding strength of the aluminum coatings sprayed by HESP and FS are shown in Fig. 8. The microhardness values of the aluminum coatings sprayed by HESP and FS are 50.8 HV_{0.1} and 34.4 HV_{0.1}, and the bonding strengths are 43.7 and 33.3 MPa, respectively. The mechanical properties of the aluminum coatings sprayed by HESP are better than those sprayed by FS. This is because pores, cracks, unmelted particles and other defects in the coatings have a great influence on the microhardness and bonding strength of the coatings (Ref 20-23). More voids, cracks, and unmelted particles in the coating will lead to loosening of the coatings, which will reduce their hardness and bonding strength. As can be seen from Fig. 5 and 6, aluminum coatings sprayed by FS have many pores, cracks, and unmelted particles in the coatings and there are a lot of

Fig. 5 Surface morphologies of (a) HESP-sprayed coatings and (b) FS-sprayed coatings

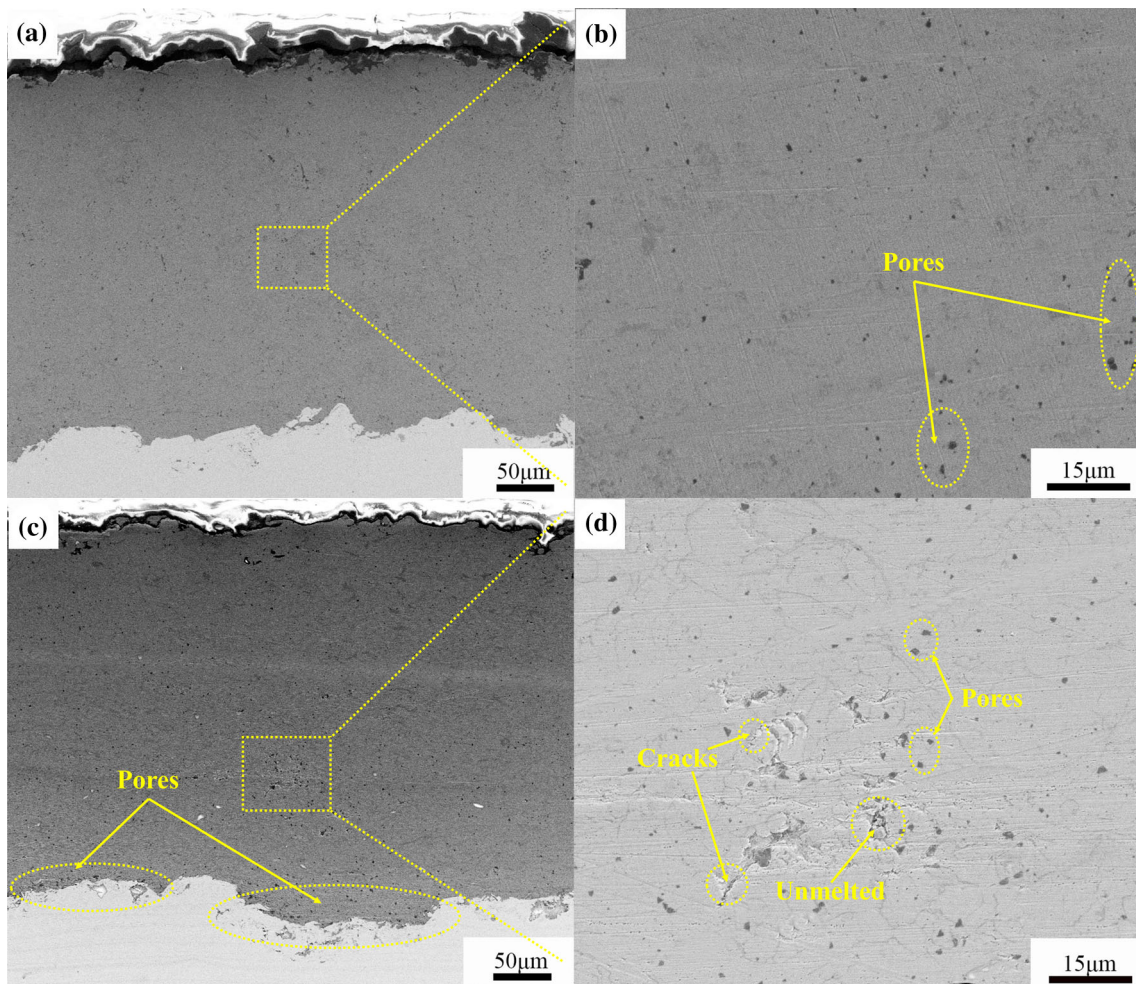
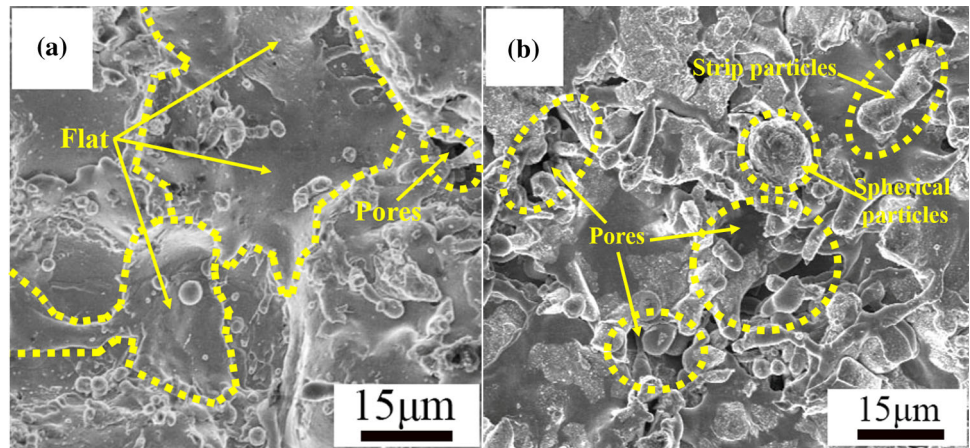


Fig. 6 Cross section morphologies of aluminum coatings: (a) HESP-sprayed coatings (low magnification), (b) HESP-sprayed coatings (high magnification), (c) FS-sprayed coatings (low magnification), and (d) FS-sprayed coatings (high magnification)

pores and cracks at the interface between coatings and substrate. On the contrary, the aluminum coatings sprayed by HESP have fewer pores, and the coating is compactly

filled on the rough surface of the substrate, which makes the microhardness and bonding strength of the aluminum coatings sprayed by HESP higher than that sprayed by FS.

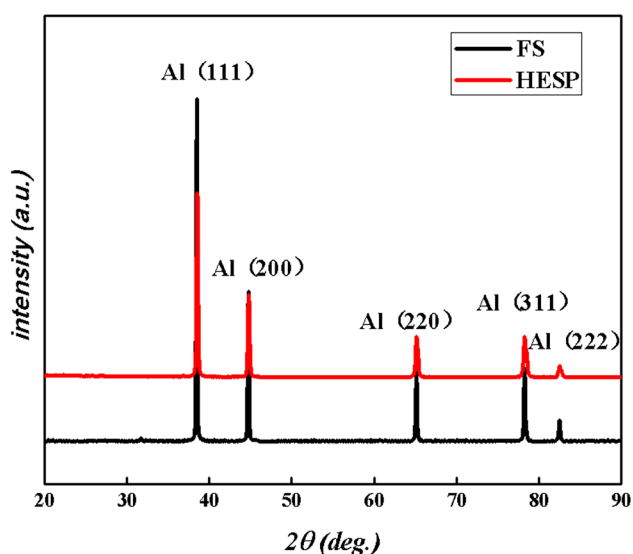


Fig. 7 X-ray diffraction pattern of aluminum coatings

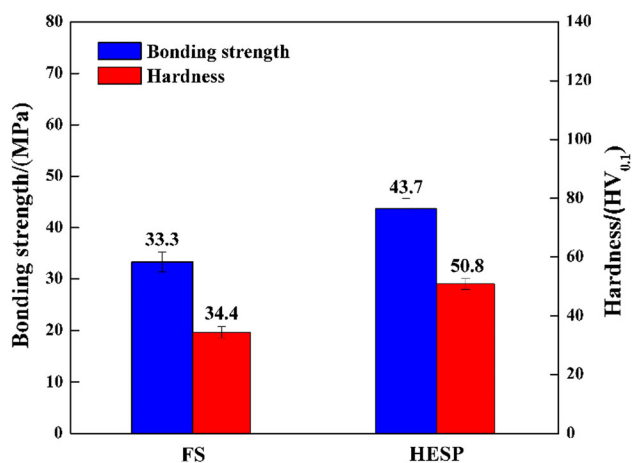


Fig. 8 Microhardness and bonding strength of aluminum coatings

Corrosion Resistance of Aluminum Coatings

Potentiodynamic Studies of Aluminum Coatings

Figure 9 shows the potentiodynamic polarization curves of the aluminum coatings sprayed by HESP and FS in 3.5 wt.% NaCl solution at room temperature. The values of corrosion potential (E_{corr}), corrosion current density (I_{corr}), and polarization resistance (R_p) were fitted from the curves in the Tafel region (Table 2). The E_{corr} of the aluminum coatings sprayed by HESP and FS are -0.91 and -1.03 V, respectively, which are lower than that (-0.61 V) of mild steel (Ref 24). This indicates that the aluminum coatings have a good cathodic protection effect on mild steel. The E_{corr} of the aluminum coatings sprayed by HESP is higher than that of FS, which is due to the presence of fewer surface defects of aluminum coatings

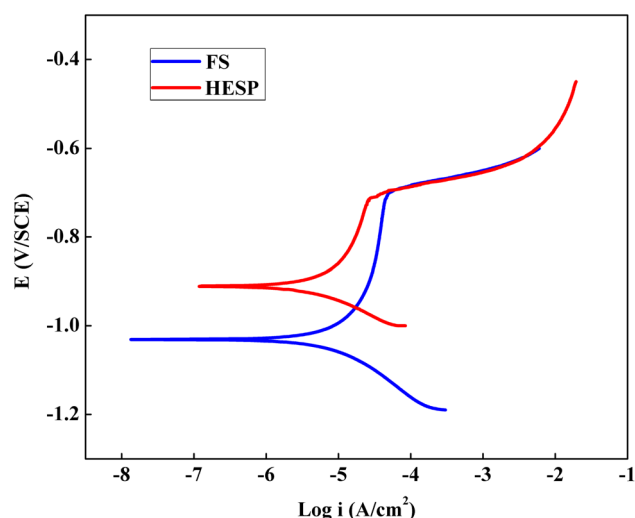


Fig. 9 Potentiodynamic polarization curves of aluminum coatings

sprayed by HESP, resulting in less surface activity of the coating before corrosion. A higher E_{corr} indicates less corrosion tendency. The I_{corr} of the aluminum coatings sprayed by HESP and FS is 4.62×10^{-6} A/cm² and 1.54×10^{-5} A/cm², respectively. The I_{corr} reflects corrosion rate to some extent, and the higher the I_{corr} , the faster the corrosion rate. The I_{corr} of aluminum coatings sprayed by FS is an order of magnitude higher than that sprayed by HESP, so the corrosion tendency of HESP coating is less.

The R_p of the aluminum coatings sprayed by HESP and FS is 14,691 (Ω cm²) and 3170 (Ω cm²), respectively. These results show that the aluminum coatings sprayed by HESP have higher E_{corr} and R_p and lower I_{corr} than those sprayed by FS, which can provide better protection for mild steel.

EIS Studies of Aluminum Coatings

EIS is a very useful technique for determining the corrosion characteristics of the interface between solution and coatings. The corrosion resistance of aluminum coatings immersed in 3.5 wt.% NaCl solution for different time periods was evaluated by EIS.

Figure 10(a) and (b) shows Nyquist plots of the aluminum coatings sprayed by HESP and FS. Before being immersed in 3.5 wt.% NaCl solution (0.5 h), there was one

Table 2 Corrosion potential, corrosion current density, and polarization resistance of aluminum coatings

	E_{corr} (V)	I_{corr} (A/cm ²)	R_p (Ω cm ²)
HESP	-0.91	$4.62\text{E}-6$	14,691
FS	-1.03	$1.54\text{E}-5$	3170

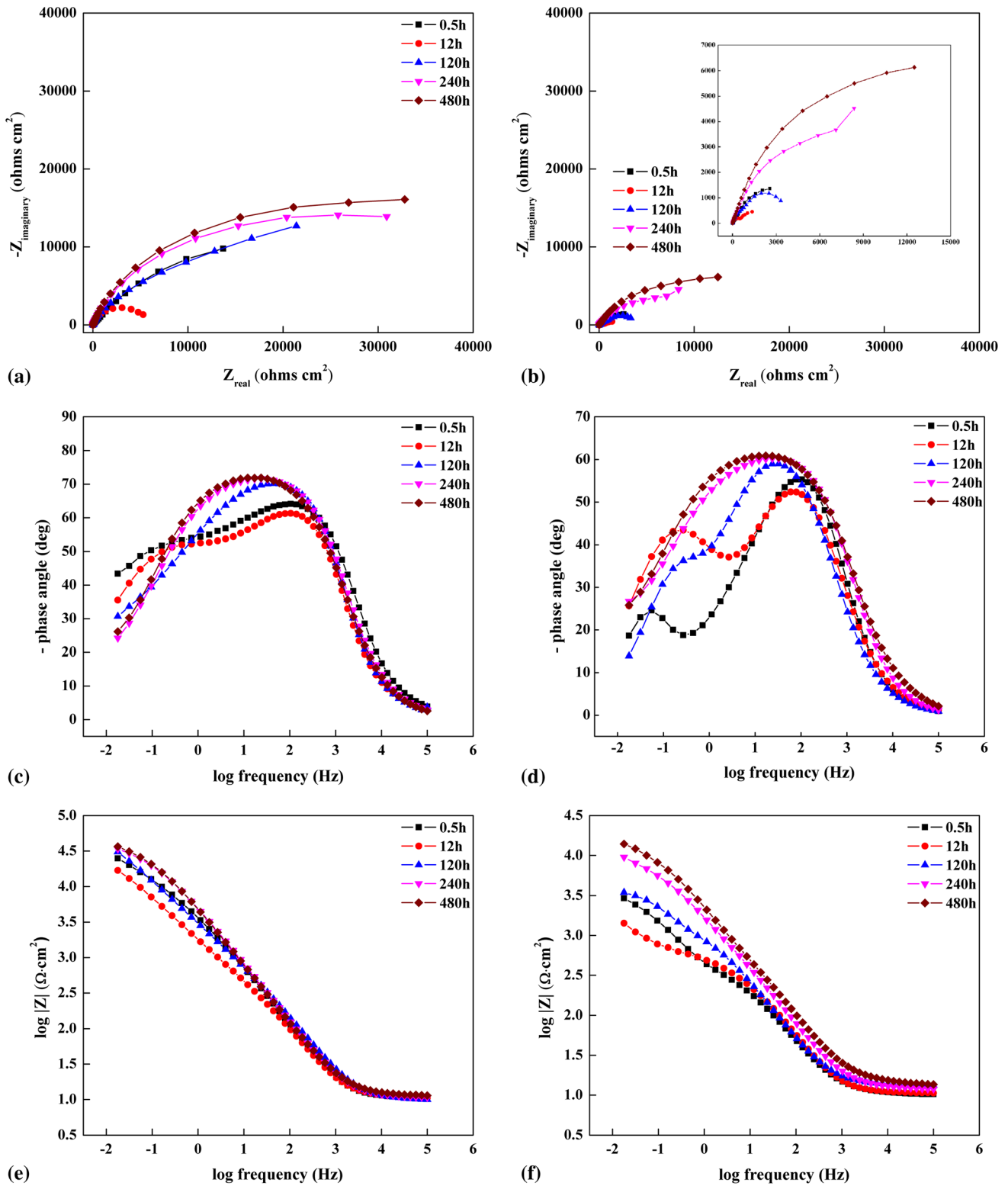


Fig. 10 EIS pattern of aluminum coatings: (a) Nyquist plot of HESP-sprayed coatings, (b) Nyquist plot of FS-sprayed coatings, (c) Bode phase plot of HESP-sprayed coatings, (d) Bode phase plot of FS-

sprayed coatings, (e) impedance modulus plot of HESP-sprayed coatings, and (f) impedance modulus plot of FS-sprayed coatings

capacitive loop that formed. This is because the surface of the coatings is polished by #1500 SiC water sandpaper before immersion. Thus, the surface of the coatings is smooth and compact, with low roughness and high surface activity, and a very thin oxide film will be formed. In 3.5 wt.% NaCl solution, this oxide film will slow down the penetration of solution into the coatings. After 12 h immersion in 3.5 wt.% NaCl solution, the diameter of capacitive loop drastically decreased, which indicated that local corrosion occurred when solution penetrated into the interior of the coatings through the pores on the surface of the coating. From 120 to 480 h, the diameter of capacitive loop was significant increased compared to that of 0.5 h, which is due to the formation of corrosion products on the coatings with the corrosion proceeding. With the increase in immersion time and the accumulation of corrosion products, more corrosion products fill the surface pores and other defects of the coatings, thus slowing down the corrosion rate and the diameter of capacitive loop of 480 h is the maximum. In the Nyquist plot, the larger the diameter of the capacitive loop, the better the corrosion resistance (Ref 25). As can be seen from Fig. 10(a) and (b), the capacitive loop of the aluminum coatings sprayed by HESP is greater than that sprayed by FS.

Figure 8(c) and (d) shows Bode phase plots of the aluminum coatings sprayed by HESP and FS. From 0.5 to 12 h, there are two times constant in the Bode phase plots, and it can be described by different frequency ranges. The high-frequency capacitive loop corresponds to the coatings, which is caused by solution resistance; the low-frequency capacitive loop corresponds to the corrosion process, which is caused by capacitance (Ref 26, 27). The capacitance might be due to the formation of a very thin corrosion layer on the surface of coatings. As can be seen from Fig. 10(c) and (d), from 0.5 to 12 h, the phase angle decreases. At the same time, it can be seen from Fig. 10(e) and (f) that the impedance modulus decreases, indicating corrosion occurred on the interface between solution and coatings. Once corrosion occurs, corrosion products will form on the coating surface.

With the increase in immersion time, from 120 to 480 h, the phase angle shifted to a lower frequency, which indicated the accumulation of corrosion products and the formation of passive film. After 120 h, there is one times

constant in the Bode phase plots, and the impedance modulus is increasing in the impedance modulus plots. This indicates that a thick passive layer is formed on the surface of the coating, hindering the penetration of solution into the coatings and protecting the surface for further corrosion. The impedance modulus depicts the corrosion resistance of coatings. The larger the impedance modulus is, the better the corrosion resistance (Ref 28). It can be seen from Fig. 10(e) and (f) that the impedance modulus of the aluminum coatings sprayed by HESP is larger than that sprayed by FS. Therefore, the corrosion resistance of the aluminum coatings sprayed by HESP is better than that sprayed by FS.

Based on the results of EIS analysis of aluminum coatings, the equivalent circuits of different corrosion stages are fitted, as shown in Fig. 11. From 0.5 to 120 h, as the solution penetrates into the coating through defects such as pores on the surface of the coating, the interface between the solution and the coating is corroded and the coating begins to dissolve. The equivalent circuit for this period of time can be modeled in Fig. 11(a). The equivalent circuit includes a solution resistance (R_s) between the working electrode (aluminum coatings) and the reference electrode (SCE), a pair of elements of pore resistance (R_p), and a coating constant phase element (CPE_{-c}) in parallel which relates to the coatings defects, and another pair of elements of charge transfer resistance (R_{dl}) and a double-layer constant phase element (CPE_{-dl}) related to the corrosion process. Since the dissolution of the coatings and the formation of corrosion products occur simultaneously, the appearance of CPE_{-dl} is due to the formation of a double-layer capacitance between the coatings and the corrosion products. From 240 to 480 h, the equivalent circuit can be modeled in Fig. 11(b). Weber impedance appears in the equivalent circuit. Usually, when corrosion products accumulate in the pores of coatings, Weber impedance will appear, which results in mass transfer reaction (Ref 29, 30).

According to the fitted equivalent circuits, the fitted circuit parameters are shown in Table 3. From 0.5 to 120 h, with the prolongation of immersion time, the R_{dl} value and R_p value increase, and the CPE_{-c} value and CPE_{-dl} value decrease. This indicated that a thick layer of corrosion products formed on the surface of the aluminum coatings in 3.5 wt.% NaCl solution. From 240 to 480 h, Weber

Fig. 11 Equivalent circuit of corrosion process for aluminum coatings in 3.5 wt.% NaCl solution

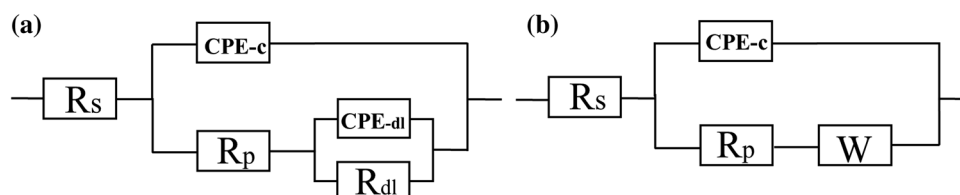


Table 3 Electrochemical parameters of aluminum coatings

	Time (h)	R_s (Ω cm ²)	CPE_{-c} (μ F/cm ²)	n	R_p (Ω cm ²)	CPE_{-dl} (μ F/cm ²)	n	R_{dl} (Ω cm ²)	W μ /(cm ² Ω s ^{0.5})
HESP	0.5	10.01	51	0.81	685	1044	0.8	1107	...
	12	10.56	43	0.85	1195	942	0.82	2532	...
	120	10.91	37	0.8	6280	765	0.84	8952	...
	240	11.3	35	0.82	10,800	560
	480	11.5	23	0.8	53,590	495
FS	0.5	10.44	144	0.8	485	2510	0.8	1842	...
	12	10.55	142	0.78	788	654	0.75	2766	...
	120	13.20	127	0.8	1152	551	0.8	2846	...
	240	11.53	122	0.73	6859	54
	480	13.40	105	0.72	13,250	50

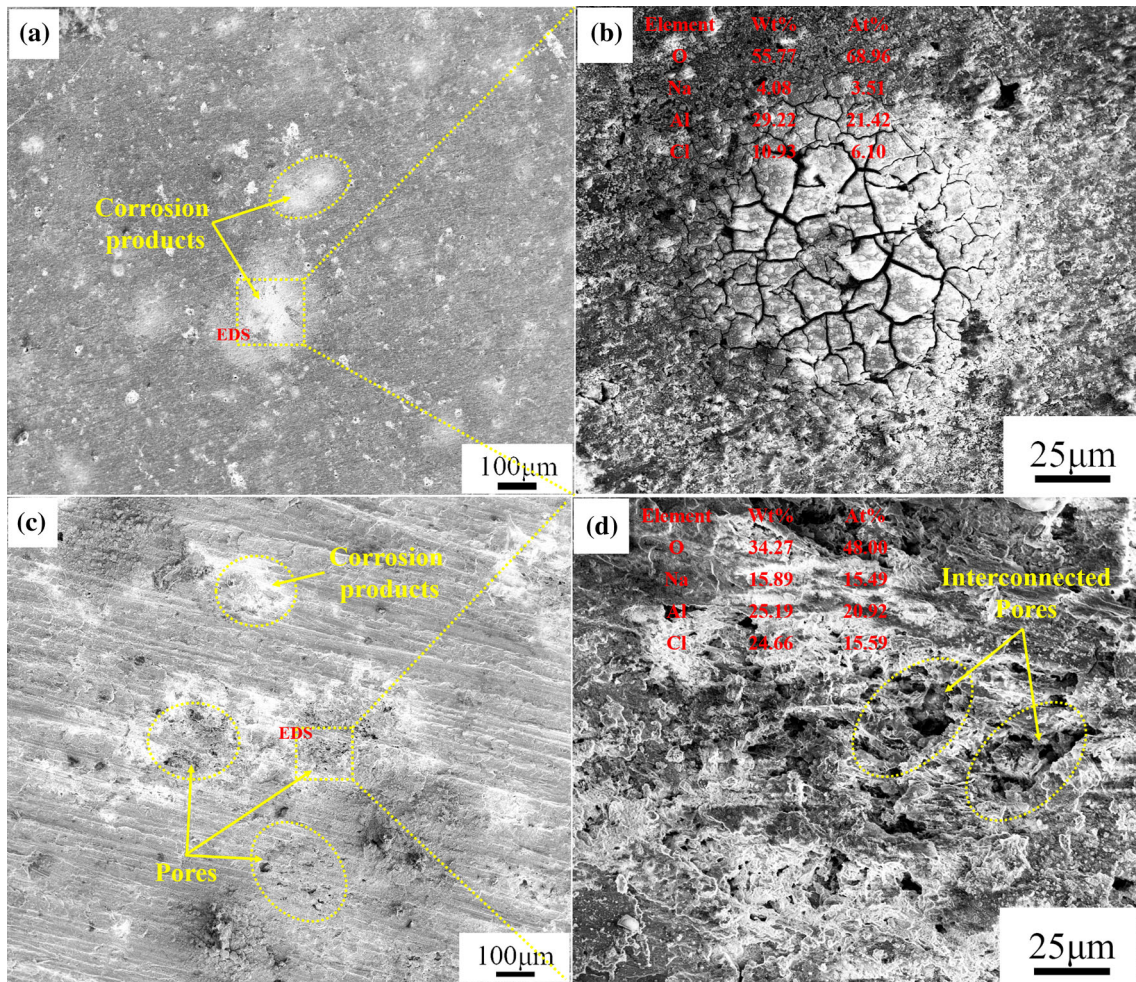


Fig. 12 Surface corrosion morphologies and EDS of aluminum coatings: (a) HESP-sprayed coatings (low magnification), (b) HESP-sprayed coatings (high magnification), (c) FS-sprayed coatings (low magnification) and (d) FS-sprayed coatings (high magnification)

impedance appeared. The phenomenon shows that the corrosion products can plug the pores and be used as a barrier to prevent the solution from penetrating into the coatings and protect the surface from further corrosion, which is the blocking effect.

Corrosion Surfaces of Aluminum Coatings

Figure 12 shows the surface corrosion morphologies and EDS analysis of the aluminum coatings sprayed by HESP and FS immersed in 3.5 wt.% NaCl solution for 480 h. As

can be seen from Fig. 12(a), the surface of the aluminum coatings sprayed by HESP is uniformly corroded, with no more corrosion holes, and dispersed with white flocs. The white flocs were analyzed by EDS, and four elements, O, Na, Al, and Cl, were detected. Cl and Na elements come from NaCl solution, and the high content of O element probably comes from the corrosion products $\text{Al}(\text{OH})_3$ (Ref 31). From the high magnification of the corrosion products in Fig. 12(b), the corrosion products are uniform, dense, and thick, which block the pores on the surface of the coatings, hinder the penetration of corrosion medium into the inside of the coatings, and protect the surface from further corrosion.

It can be seen from Fig. 12(c) that the surface of the aluminum coatings sprayed by FS is also dispersed with obvious white flocs, but there are more corrosion holes, indicating that serious pitting corrosion occurs. The EDS analysis of the holes also shows four elements O, Na, Al, and Cl, among which the content of O element was higher, indicating that corrosion products existed in the holes. However, from the high magnification of the holes in Fig. 12(d), the corrosion pores of the coating are shown to be interconnected, indicating that the corrosion is serious. This may be because the surface of the aluminum coatings sprayed by FS is rough and there are many pores. The corrosion products are not enough to plug the pores, which results in the penetration of corrosion medium into the coatings, leading to serious corrosion. So, the aluminum coatings sprayed by HESP have good quality and better corrosion resistance than that sprayed by FS.

Figure 13 shows XRD analysis of aluminum coatings sprayed by HESP after corrosion in 3.5 wt.% NaCl

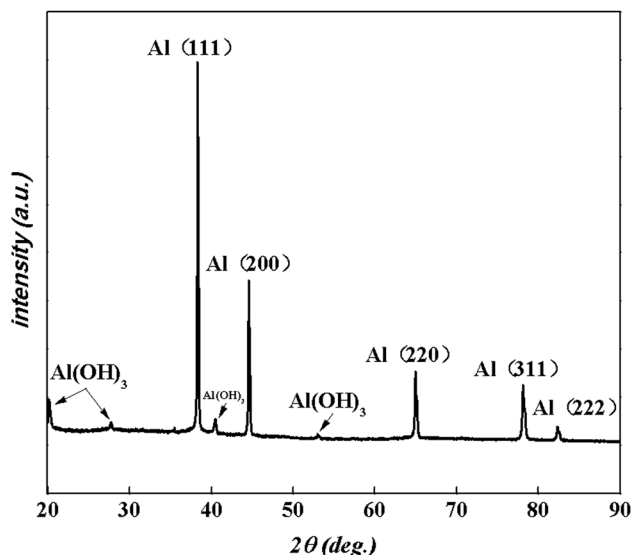


Fig. 13 X-ray diffraction pattern of aluminum coatings after corrosion in 3.5 wt.% NaCl solution

solution. The characteristic peaks of aluminum on the surface of the coatings after corrosion are the most obvious, indicating that the main component of the coatings surface is still aluminum. At the same time, the characteristic peak of $\text{Al}(\text{OH})_3$ appeared, indicating that $\text{Al}(\text{OH})_3$ was formed on the coating, which further indicated that the white flocs were the corrosion product $\text{Al}(\text{OH})_3$.

Conclusions

From the above results, the following main conclusions can be drawn:

1. The aluminum coatings sprayed by HESP are denser than those sprayed by FS, which is attributed to the inert spraying heat source and supersonic speed of HESP. The sprayed particles can be fully deformed and spread when they reach the substrate. The porosities of the aluminum coatings sprayed by HESP and FS are 1.02 and 2.18%, respectively.
2. The mechanical properties of the aluminum coatings sprayed by HESP are better than those sprayed by FS, which is attributed to fewer defects of aluminum coatings sprayed by HESP. The microhardness values of the aluminum coatings sprayed by HESP and FS are 50.8 $\text{HV}_{0.1}$ and 34.4 $\text{HV}_{0.1}$, and the bonding strengths between coatings and substrate are 43.7 and 33.3 MPa, respectively.
3. Potentiodynamic and EIS studies reveal kinetics of protective properties of aluminum coatings in 3.5 wt.% NaCl solution with different exposure periods. Compared with the aluminum coatings sprayed by FS, the aluminum coatings sprayed by HESP show a larger capacitive loop, phase angle, and impedance modulus, indicating that the aluminum coatings sprayed by HESP possess better corrosion resistance than those sprayed by FS.
4. After 480-h immersion in 3.5 wt.% NaCl solution, a dense corrosion product formed on the surface of aluminum coatings sprayed by HESP prevents further corrosion of the coatings. However, the aluminum coatings sprayed by FS exhibit serious pitting corrosion.

Acknowledgments This work was supported by the National Natural Science Foundation of China (Grant Nos. 51535011, 41872183, 51675531), the Pre-Research Program in National 13th Five-Year Plan (Grant No. 61409230603), Joint Fund of Ministry of Education for Pre-research of Equipment for Young Personnel Project (Grant No. 6141A02033120), and the Fundamental Research Funds for Central Universities (Grant No. 2652018095).

References

1. H. Katayama and S. Kuroda, Long-term Atmospheric Corrosion Properties of Thermally Sprayed Zn, Al and Zn-Al Coatings Exposed in a Coastal Area, *Corros. Sci.*, 2013, **76**, p 35-41
2. S. Paul, Corrosion Performance of Damaged Thermally Sprayed Aluminum in Synthetic Seawater at Different Temperatures, *Therm. Spray Bull.*, 2015, **8**, p 139-146
3. H.S. Lee, J.K. Singh, and J.H. Park, Pore Blocking Characteristics of Corrosion Products Formed on Aluminum Coating Produced by Arc Thermal Metal Spray Process in 3.5wt.% NaCl Solution, *Constr. Build. Mater.*, 2016, **113**, p 905-916
4. X.B. Liu, J.J. Kang, W. Yue, G.Z. Ma, Z.Q. Fu, L.N. Zhu, D.S. She, J. Liang, W. Weng, H.D. Wang, and C.B. Wang, Cavitation Erosion Behavior of HVOF Sprayed WC-10Co4Cr Cermet Coatings in Simulated Sea Water, *Ocean Eng.*, 2019, **190**, p 106449. <https://doi.org/10.1016/j.oceaneng.2019.106449>
5. F. Ahnia and B. Demri, Evaluation of Aluminum Coatings in Simulated Marine Environment, *Surf. Coat. Technol.*, 2013, **220**, p 232-236
6. C. Jeong, J. Lee, K. Sheppard, and C.H. Choi, Air-Impregnated Nanoporous Anodic Aluminum Oxide Layers for Enhancing the Corrosion Resistance of Aluminum, *Langmuir*, 2015, **31**, p 11040-11050
7. Q. Jiang, Q. Miao, W.P. Liang, F. Ying, F. Tong, Y. Xu, B.L. Ren, Z.J. Yao, and P.Z. Zhang, Corrosion Behavior of Arc Sprayed Al-Zn-Si-RE Coatings on Mild Steel in 3.5wt% NaCl Solution, *Electrochim. Acta*, 2014, **115**, p 644-656
8. E.A. Esfahani, H. Salimijazi, M.A. Golozar, J. Mostaghimi, and L. Pershln, Study of Corrosion Behavior of Arc Sprayed Aluminum Coating on Mild Steel, *J. Therm. Spray Technol.*, 2012, **21**, p 1195-1202
9. X.B. Zhang, X. Chang, F.H. Han, and W.J. Huang, Researches on Aluminum Coating by Flame Spraying on Q235 Steel Surface, *Adv. Mater. Res.*, 2012, **472-475**, p 2775-2778
10. L. Pawlowski, *The Science and Engineering of Thermal Spray Coatings*, 2nd ed., Wiley-Blackwell Press, Hoboken, 2008
11. G. Zlatko, K. Zoran, and K. Slobodan, A Mathematical Model for the Calculation of the Adhesion of a Flame Sprayed Coating of Aluminum on S 235 JR Steel, *J. Therm. Spray Technol.*, 2012, **21**(1), p 63-76
12. M.H.A. Malek, N.H. Saad, S.K. Abas, N.R.N. Roselina, and N.M. Shah, Performance and Microstructure Analysis of 99.5% Aluminum Coating by Thermal Arc Spray Technique, *Procedia Eng.*, 2013, **68**, p 558-565
13. R.M.H.P. Rodriguez, R.S.C. Paredes, S.H. Wido, and A. Calixto, Comparison of Aluminum Coatings Deposited by Flame Spray and by Electric Arc Spray, *Surf. Coat. Technol.*, 2007, **202**, p 172-179
14. R.S.C. Paredes, S.C. Amico, and A.S.C.M. D'Oliveira, The Effect of Roughness and Pre-heating of the Substrate on the Morphology of Aluminum Coatings Deposited by Thermal Spraying, *Surf. Coat. Technol.*, 2006, **200**, p 3049-3055
15. H.S. Lee, J.K. Singh, M.A. Ismail, and C. Bhattacharya, Corrosion Resistance Properties of Aluminum Coating Applied by Arc Thermal Metal Spray in SAE J2334 Solution with Exposure Periods, *Metals*, 2016, **6**, p 55-70
16. H.B. Choe, H.S. Lee, and J.H. Shin, Experimental Study on the Electrochemical Anti-corrosion Properties of Steel Structures Applying the Arc Thermal Metal Spraying Method, *Materials*, 2014, **7**, p 7722-7736
17. H.S. Lee, J.K. Singh, and M.A. Ismail, An effective and Novel Pore Sealing Agent to Enhance the Corrosion Resistance Performance of Al Coating in Artificial Ocean Water, *Sci. Rep.*, 2017, **7**, p 41935. <https://doi.org/10.1038/srep41935>
18. H.S. Lee, J.H. Park, J.K. Singh, and M.A. Ismail, Protection of Reinforced Concrete Structures of Waste Water Treatment Reservoirs with Stainless Steel Coating Using Arc Thermal Spraying Technique in Acidified Water, *Materials*, 2016, **9**, p 753-773
19. Z.A. Jin, L.N. Zhu, H.D. Wang, M. Liu, J.J. Kang, G.Z. Ma, and S.Y. Chen, Microstructures and Wear Resistance of Al-25wt.%Si Coatings Prepared by High-Efficiency Supersonic Plasma Spraying, *J. Therm. Spray Technol.*, 2019, **28**(6), p 1308-1317
20. M.S. Han, Y.B. Woo, S.C. Ko, Y.J. Jeong, S.K. Jang, and S.J. Kim, Effects of Thickness of Al Thermal Spray Coating for STS 304, *Trans. Nonferrous Met. Soc. China*, 2009, **19**, p 925-929
21. S.J. Kim and Y.B. Woo, Coating Layer and Corrosion Protection Characteristics in Sea Water with Various Thermal Spray Coating Materials for STS304, *Surf. Rev. Lett.*, 2010, **17**, p 299-305
22. W.B. Qin, J.S. Li, Y.Y. Liu, J.J. Kang, L.N. Zhu, D.F. Shu, P. Peng, D.S. She, D.Z. Meng, and Y.S. Li, Effects of Grain Size on Tensile Property and Fracture Morphology of 316L Stainless Steel, *Mater. Lett.*, 2019, **254**, p 116-119
23. L. Tang, J.J. Kang, P.F. He, S.Y. Ding, S.Y. Chen, M. Liu, Y.C. Xiong, G.Z. Ma, and H.D. Wang, Effects of Spraying Conditions on the Microstructure and Properties of NiCrBSi Coatings Prepared by Internal Rotating Plasma Spraying, *Surf. Coat. Technol.*, 2019, **374**, p 625-633
24. C.J. Li and A. Ohmori, Relationships Between the Microstructure and Properties of Thermally Sprayed Deposits, *J. Therm. Spray Technol.*, 2002, **11**, p 365-374
25. M.M. Verdian, K. Raeissi, and M. Salehi, Corrosion Performance of HVOF and APS Thermally Sprayed NiTi Intermetallic Coatings in 3.5 wt.% NaCl Solution, *Corros. Sci.*, 2010, **52**, p 1052-1059
26. J.L. Ma, J.B. Wen, G.X. Li, and C.H. Xu, The Corrosion Behaviour of Al-Zn-In-Mg-Ti Alloy in NaCl Solution, *Corros. Sci.*, 2010, **52**, p 534-539
27. R. Autengruber, G. Luckeneder, and A.W. Hassel, Corrosion of Press-Hardened Galvanized Steel, *Corros. Sci.*, 2012, **63**, p 12-19
28. J.B. Wen, J.L. Ma, and J.G. He, *Al-Base Sacrificial Anode Material for Corrosion Protection*, Chemical Industry Press, Beijing, 2012
29. J.F. Zhang, W. Zhang, C.W. Yan, K.Q. Du, and F.H. Wang, Corrosion Behaviors of Zn/Al-Mn Alloy Composite Coatings Deposited on Magnesium Alloy AZ31B (Mg-Al-Zn), *Electrochim. Acta*, 2009, **55**, p 560-571
30. Y. Wang, W. Tian, T. Zhang, and Y. Yang, Microstructure, Spallation and Corrosion of Plasma Sprayed Al₂O₃-13%TiO₂ Coatings, *Corros. Sci.*, 2009, **51**, p 2924-2931
31. L.M. Liu, Z. Wang, and G. Song, Study on Corrosion Resistance Properties of Hydrothermal Sealed Arc Sprayed Aluminum Coating, *Surf. Eng.*, 2010, **26**, p 399-406

Publisher's Note Springer Nature remains neutral with regard to jurisdictional claims in published maps and institutional affiliations.